

Detection of Carbohydrates and Steroids by Cation-Enhanced Nanostructure-Initiator Mass Spectrometry (NIMS) for Biofluid Analysis and Tissue Imaging

Gary J. Patti,[†] Hin-Koon Woo,[†] Oscar Yanes,[†] Leah Shriver,[‡] Diane Thomas,[‡] Wilasinee Uritboonthai,[†] Junefredo V. Apon,[†] Rick Steenwyk,[§] Marianne Manchester,[‡] and Gary Siuzdak^{*,†}

Department of Molecular Biology, Scripps Center for Mass Spectrometry, The Scripps Research Institute, 10550 North Torrey Pines Road, La Jolla, California 92037, and Department of Cell Biology, The Scripps Research Institute, 10550 North Torrey Pines Road, La Jolla, California 92037

Nanostructure-initiator mass spectrometry (NIMS) is a highly sensitive, matrix-free technique that is well suited for biofluid analysis and imaging of biological tissues. Here we provide a new technical variation of NIMS to analyze carbohydrates and steroids, molecules that are challenging to detect with traditional mass spectrometric approaches. Analysis of carbohydrates and steroids was accomplished by spray depositing NaCl or AgNO₃ on the NIMS porous silicon surface to provide a uniform environment rich with cationization agents prior to desorption of the fluorinated polymer initiator. Laser desorption/ionization of the ion-coated NIMS surface allowed for Na⁺ cationization of carbohydrates and Ag⁺ cationization of steroids. The reliability of the approach is quantitatively demonstrated with a calibration curve over the physiological range of glucose and cholesterol concentrations in human serum (1–200 μM). Additionally, we illustrate the sensitivity of the method by showing its ability to detect carbohydrates and steroids down to the 800-amol and 100-fmol levels, respectively. The technique developed is well suited for tissue imaging of biologically significant metabolites such as sucrose and cholesterol. To highlight its applicability, we used cation-enhanced NIMS to image the distribution of sucrose in a *Gerbera jamesonii* flower stem and the distribution of cholesterol in a mouse brain. The flower stem and brain sections were placed directly on the ion-coated NIMS surface without further preparation and analyzed directly. The overall results reported underscore the potential of NIMS to analyze and image chemically diverse compounds that have been traditionally challenging to observe with mass spectrometry-based techniques.

Mass spectrometry imaging (MSI) is emerging as a powerful technique to probe the distribution of molecules within biological

systems.^{1–3} The molecular specificity of MSI offers significant advantages over traditional imaging techniques such as fluorescence microscopy, electron microscopy, and radiography. MSI has proven important to understanding tumor pathology,⁴ biomarkers,^{5,6} drug distribution,^{7–9} and changes in the chemical organization of tissues under a variety of therapeutic conditions.^{10–12} The applicability of MSI depends largely upon several parameters including sample preparation, method of ionization, sensitivity, resolution, and speed of the analysis. Various MSI strategies have been employed including matrix-assisted laser desorption/ionization (MALDI),^{1,13,14} atmospheric pressure-MALDI (AP-MALDI),^{15,16} time-of-flight secondary ion mass spectrometry (TOF-SIMS),^{2,17,18} desorption electrospray ionization (DESI),^{8,19} and laser ablation

- (1) Chaurand, P.; Schwartz, S. A.; Caprioli, R. M. *Curr. Opin. Chem. Biol.* **2002**, *6*, 676–681.
- (2) Ostrowski, S. G.; Szakal, C.; Kozole, J.; Roddy, T. P.; Xu, J. Y.; Ewing, A. G.; Winograd, N. *Anal. Chem.* **2005**, *77*, 6190–6196.
- (3) McDonnell, L. A.; Heeren, R. M. A. *Mass Spectrom. Rev.* **2007**, *26*, 606–643.
- (4) Chaurand, P.; Rahman, M. A.; Hunt, T.; Mobley, J. A.; Gu, G.; Latham, J. C.; Caprioli, R. M.; Kasper, S. *Mol. Cell. Proteomics* **2008**, *7*, 411–423.
- (5) Rohner, T. C.; Staab, D.; Stoekli, M. *Mech. Ageing Dev.* **2005**, *177*–185.
- (6) Rubakhin, S. S.; Jurchen, J. C.; Monroe, E. B.; Sweedler, J. V. *Drug Discov. Today* **2005**, *10*, 823–837.
- (7) Hsieh, Y.; Casale, R.; Fukuda, E.; Chen, J. W.; Knemeyer, I.; Wingate, J.; Morrison, R.; Korfmacher, W. *Rapid Commun. Mass Spectrom.* **2006**, *20*, 965–972.
- (8) Wiseman, J. M.; Ifa, D. R.; Zhu, Y. X.; Kissinger, C. B.; Manicke, N. E.; Kissinger, P. T.; Cooks, R. G. *Proc. Natl. Acad. Sci. U.S.A.* **2008**, *105*, 18120–18125.
- (9) Yanes, O.; Woo, H. K.; Northen, T. R.; Oppenheimer, S. R.; Shriver, L.; Apon, J.; Estrada, M. N.; Potchoiba, M. J.; Steenwyk, R.; Manchester, M.; Siuzdak, G. *Anal. Chem.* **2009**, *81*, 2969–2975.
- (10) Choudhury, A.; Dominguez, M.; Puri, V.; Sharma, D. K.; Narita, K.; Wheatley, C. L.; Marks, D. L.; Pagano, R. E. *J. Clin. Invest.* **2002**, *109*, 1541–1550.
- (11) Jackson, S. N.; Wang, H. Y. J.; Woods, A. S. *Anal. Chem.* **2005**, *77*, 4523–4527.
- (12) Khatib-Shahidi, S.; Andersson, M.; Herman, J. L.; Gillespie, T. A.; Caprioli, R. M. *Anal. Chem.* **2006**, *78*, 6448–6456.
- (13) Karas, M.; Hillenkamp, F. *Anal. Chem.* **1988**, *60*, 2299–2301.
- (14) Hillenkamp, F.; Karas, M.; Beavis, R. C.; Chait, B. T. *Anal. Chem.* **1991**, *63*, A1193–A1202.
- (15) Li, Y.; Shrestha, B.; Vertes, A. *Anal. Chem.* **2007**, *79*, 523–532.
- (16) Koestler, M.; Kirsch, D.; Hester, A.; Leisner, A.; Guenther, S.; Spengler, B. *Rapid Commun. Mass Spectrom.* **2008**, *22*, 3275–3285.
- (17) Sjovall, P.; Lausmaa, J.; Johansson, B. *Anal. Chem.* **2004**, *76*, 4271–4278.

* Corresponding author. Phone: (858) 784-9415. Fax: (858) 784-9496. E-mail: siuzdak@scripps.edu.

[†] Department of Molecular Biology, Scripps Center for Mass Spectrometry.

[‡] Department of Cell Biology.

[§] Present address: Pfizer Global Research and Development.

electrospray ionization (LAESI).^{20,21} While each technique offers unique advantages, MALDI is currently the most commonly used imaging approach.

MALDI has been used to image organic compounds, peptides, proteins, drugs, and metabolites.^{1,5,6,12,22} In typical MALDI experiments, the analyte is mixed and cocrystallized with an organic matrix that absorbs ultraviolet (UV) energy. Although the detailed desorption/ionization mechanism is not clear, it is generally believed that the matrix transfers energy from the laser to the analyte, thereby inducing desorption and ionization.²³ The requirement of an organic matrix, however, greatly limits the application of MALDI for the detection of small molecules given the background interference of matrix molecules at low-mass range. As a result, MALDI is rarely used for the analysis of low-molecular-weight analytes (<500 Da). Additionally, the quality of MALDI images greatly depends on the matrix-deposition method and the uniformity of the coating. A variety of matrix-application techniques have been developed to achieve homogeneous coating,^{24–26} but these methods require extra sample preparation time and expensive instrumentation.

Nanostructure-initiator mass spectrometry (NIMS) is a newly developed matrix-free technique for surface-based analysis that extends the observable mass range to small molecules not readily detectable by MALDI.²⁷ The application of NIMS to tissue imaging has recently been demonstrated using a nanostructured silicon surface to trap initiator materials that adsorb the analytes to their surface. The analytes are then desorbed by laser irradiation.⁹ NIMS is a “soft” ionization method that allows direct characterization of a wide range of biological molecules, fluids, and tissues with little or no analyte degradation. Advantages of NIMS that make it especially attractive for imaging include the absence of a matrix, high sensitivity, low background, minimal sample preparation, and flexibility in irradiation sources (e.g., laser or ion).

Carbohydrates and steroids are biologically important classes of molecules that are difficult to observe by current surface-based MS methods as a result of their poor ionization efficiency.^{28–30} The most effective approach to detect carbohydrates with MALDI has been with the use of 2,5-dihydroxybenzoic acid (DHB) matrix, but inhomogeneous cocrystallization of the analytes and matrix generally results in substantial shot-to-shot variability. Further-

more, the matrix interferes with the detection of important low-mass carbohydrates like glucose, sucrose, and maltotriose.

Alternatively, chemical derivatization strategies such as permethylation and sulfation have been used to enhance MS detection of carbohydrates and steroids, respectively.^{29,31–34} For steroids, chemical derivatization approaches are traditionally used with gas chromatography/MS (GC/MS).^{35–37} Although GC/MS has proven successful for the analysis of some steroids, chemical preparation is time-consuming and the derivatization process depends on the individual properties of the steroids. Thus, other ionization techniques (like atmospheric pressure chemical ionization or atmospheric pressure photoionization) have also been used to analyze intact steroids without derivatization.^{38–40} However, these approaches do not readily allow for MS imaging.

In this report, we describe a new MS method combining spray deposition and NIMS to detect carbohydrates and steroids without sample derivatization. The method was implemented to quantify the concentration of glucose and cholesterol in human serum. We then show the application of our approach to image the sucrose distribution in a *Gerbera jamesonii* flower stem and cholesterol distribution in a mouse brain.

EXPERIMENTAL SECTION

Materials. Glucose, glucose ¹³C₆, sucrose, maltotriose, maltohexaose (G6), maltoheptaose (G7), β-, γ-cyclodextrins, cholesterol, ergosterol, trans-androsterone, progesterone, corticosterone, prednisone, human serum, NaCl, AgNO₃, ethanol, acetonitrile, chloroform, and formic acid were purchased from Sigma-Aldrich (St. Louis, MO). Hydrofluoric acid (HF) and methanol were purchased from Fisher Scientific (Fair Lawn, NJ) with the highest purity available. Nanopure water was obtained from a Millipore water purification system (Millipore, Bedford, MA) with a resistivity more than 18 MΩ cm.

Initiator Materials. Bis(heptadecafluoro-1,1,2,2-tetrahydrodecyl)tetramethyldisiloxane (BisF17) and 3-aminopropyltrimethylethoxysilane (APDMES) were obtained from Gelest (Morrisville, PA).

Preparation of NIMS Surfaces. A detailed description of the preparation of NIMS surfaces is reported elsewhere.⁴¹ Briefly, single-side polished p-type (100) silicon wafers (500–550 μm thick) with low resistivity (0.01–0.02 Ω cm) were obtained from Silicon Quest International (Santa Clara, CA) and cut into 3.3 cm × 3.3 cm pieces. The pieces were then soaked in a mixture of sulfuric acid and hydrogen peroxide (piranha) solution (2:1) for 30 min. The chips were rinsed by nanopure water and blown dry with

- (18) Altelaar, A. F. M.; van Minnen, J.; Jimenez, C. R.; Heeren, R. M. A.; Piersma, S. R. *Anal. Chem.* **2005**, *77*, 735–741.
- (19) Wiseman, J. M.; Ifa, D. R.; Song, Q. Y.; Cooks, R. G. *Angew. Chem., Int. Ed.* **2006**, *45*, 7188–7192.
- (20) Nemes, P.; Barton, A. A.; Li, Y.; Vertes, A. *Anal. Chem.* **2008**, *80*, 4575–4582.
- (21) Nemes, P.; Vertes, A. *Anal. Chem.* **2007**, *79*, 8098–8106.
- (22) Liu, Q.; Xiao, Y. S.; Pagan-Miranda, C.; Chiu, Y. M.; He, L. *J. Am. Soc. Mass Spectrom.* **2009**, *20*, 80–88.
- (23) Zenobi, R.; Knochenmuss, R. *Mass Spectrom. Rev.* **1998**, *17*, 337–366.
- (24) Hankin, J. A.; Barkley, R. M.; Murphy, R. C. *J. Am. Soc. Mass Spectrom.* **2007**, *18*, 1646–1652.
- (25) Puolitaival, S. M.; Burnum, K. E.; Cornett, D. S.; Caprioli, R. M. *J. Am. Soc. Mass Spectrom.* **2008**, *19*, 882–886.
- (26) Chen, Y. F.; Allegood, J.; Liu, Y.; Wang, E.; Cachon-Gonzalez, B.; Cox, T. M.; Merrill, A. H.; Sullards, M. C. *Anal. Chem.* **2008**, *80*, 2780–2788.
- (27) Northen, T. R.; Yanes, O.; Northen, M. T.; Marrinucci, D.; Uritboonthai, W.; Apon, J.; Golledge, S. L.; Nordstrom, A.; Siuzdak, G. *Nature* **2007**, *449*, 1033–U1033.
- (28) Harvey, D. *J. Mass Spectrom. Rev.* **1999**, *18*, 349–450.
- (29) Compton, B. J.; Siuzdak, G. *Spectroscopy* **2003**, *17*, 699–713.
- (30) Kauppila, T. J.; Talaty, N.; Jackson, A. U.; Kotiaho, T.; Kostianen, R.; Cooks, R. G. *Chem. Commun.* **2008**, 2674–2676.

- (31) Chatman, K.; Hollenbeck, T.; Hagey, L.; Vallee, M.; Purdy, R.; Weiss, F.; Siuzdak, G. *Anal. Chem.* **1999**, *71*, 2358–2363.
- (32) Harvey, D. *J. Int. J. Mass Spectrom.* **2003**, *226*, 1–35.
- (33) Price, N. P. *J. Anal. Chem.* **2004**, *76*, 6566–6574.
- (34) Higashi, T.; Shimada, K. *Anal. Bioanal. Chem.* **2004**, *378*, 875–882.
- (35) Wolthers, B. G.; Kraan, G. P. B. *J. Chromatogr.* **1999**, *843*, 247–274.
- (36) Shimada, K.; Mitamura, K.; Higashi, T. *J. Chromatogr.* **2001**, *935*, 141–172.
- (37) Griffiths, W. *J. Mass Spectrom. Rev.* **2003**, *22*, 81–152.
- (38) Greig, M. J.; Bolanos, B.; Quenzer, T.; Bylund, J. M. *Rapid Commun. Mass Spectrom.* **2003**, *17*, 2763–2768.
- (39) Kauppila, T. J.; Nikkola, T.; Ketola, R. A.; Kostianen, R. *J. Mass Spectrom.* **2006**, *41*, 781–789.
- (40) Haapala, M.; Luosujarvi, L.; Saarela, V.; Kotiaho, T.; Ketola, R. A.; Franssila, S.; Kostianen, R. *Anal. Chem.* **2007**, *79*, 4994–4999.
- (41) Woo, H. K.; Northen, T. R.; Yanes, O.; Siuzdak, G. *Nat. Protoc.* **2008**, *3*, 1341–1349.

nitrogen gas. Etching was performed by clamping chips between gold foil (anode) in a Teflon chamber that was subsequently filled with 25% ethanolic HF solution. A platinum loop immersed in the HF solution served as the cathode. Etchings were performed in constant-current mode (300 mA) for 30 min using a BIO-RAD PowerPack1000 power supply (Hercules, CA). Etched nanostructure silicon surfaces were rinsed with methanol and blown dry with nitrogen. The chips were stored in initiator for 30 min and then blown dry with nitrogen gas.

Mass Spectrometry and Tissue Imaging. All mass spectra and images were acquired using a MALDI time-of-flight (TOF) or MALDI-TOF/TOF mass spectrometer (Voyager DE-STR or 4800, Applied Biosystems, Foster City, CA). A nitrogen laser at 337 nm or a Nd:YAG laser at 355 nm was used. The spectra were recorded in reflection mode using an accelerating voltage of 20 kV, a 66% grid voltage, and a 50–200 ns delay extraction. Typically, 10–60 laser shots were collected per spectrum. Propafenone and bradykinin fragment 2–9 were used to calibrate the mass spectrometer in the low-mass range. Mouse brains were sectioned by using a Leica CM1850 cryostat (Leica Microsystems Inc., Germany), thaw-mounted onto NIMS chips, and stored at ambient conditions for ~30 min prior to analysis. Images were acquired using MALDI MS Imaging Tool software with a typical resolution of $75 \times 75 \mu\text{m}$. Data analysis and image reconstruction was preformed using BioMap software.

Metabolite Identification. Metabolite identifications were determined by mass (the mass accuracy of our MALDI-TOF data is <100 ppm). Identifications were confirmed by comparing the MALDI-TOF/TOF fragmentation pattern of the ion to that of an authentic model compound.

Spray Deposition. Spray deposition was performed by using a fused-silica PicoTip emitter (New Objective, Woburn, MA). A continuous supply of NaCl or AgNO₃ solution was accomplished using a syringe pump set at a flow rate of 200 to 600 $\mu\text{L}/\text{h}$ and a typical spray voltage of +2 to +3 kV. Concentrations of NaCl and AgNO₃ were 1 mg/mL and 0.5 mg/mL in 50% methanol/water solutions, respectively. A stable spray was achieved by optimizing the flow rate and voltage. Typically, 200 μL of solution was deposited on the entire NIMS surface. After the spray deposition, the NIMS chip was incubated at 90 °C for 5 min before applying the initiator.

Quantitative Analysis of Glucose and Cholesterol from Human Serum. All data analyses were performed by averaging 60 laser shots per spectrum, and each spectrum was collected at different locations within the sample spot. Data processing involved baseline correction and noise filtering. Quantitative analysis was performed using the standard-addition method. Calibration curves were constructed by plotting the peak intensity of the analyte to the internal standard versus the concentration of the spiked analyte. All calibration curves were fitted to a nonweighted linear regression, and standard deviations were calculated by 10 individual measurements. Both glucose and cholesterol showed similar variation in the concentration range 1–200 μM . The coefficient of variation over this concentration range was determined to be 15% from 3 replicates measured on different days. We observed higher variation with increasing analyte concentration.

Preparation of *Gerbera jamesonii* Stems and Mouse Tissues. *Gerbera jamesonii* flowers were purchased from a local florist. A small piece of stem was cut with a razor blade and snap frozen in OCT compound-embedding medium (VWR International, West Chester, PA) on dry ice, equilibrated to $-20\text{ }^\circ\text{C}$, sectioned to 3–5 μm , and deposited on the NIMS surface. Adult male mice (Balb/cByJ) were obtained from The Scripps Research Institute Rodent Breeding Colony and maintained according to the Institutional Animal Care and Use Committee (IACUC) approved protocols. Mice were deeply anesthetized by isoflurane inhalation and sacrificed by cervical dislocation. Brains were collected, snap frozen in OCT compound-embedding medium on dry ice, equilibrated to $-20\text{ }^\circ\text{C}$, sectioned to 3–5 μm , and deposited on a NIMS surface. All procedures were approved by the IACUC at The Scripps Research Institute and conform to the National Institutes of Health guidelines.

Safety Considerations. Piranha solution is highly reactive and can become extremely hot when prepared; it is corrosive and irritating to the eyes, skin, and respiratory tract. When working with piranha solution, it is recommended that one always use glass containers as Piranha can melt plastic. We prepared piranha solutions by adding peroxide to acid (violating the “add acid to water” rule), adding the peroxide solution very slowly while mixing the solution with a clean Pasteur pipet or glass rod. When mixing the solutions, one should be in a ventilated fume hood wearing gloves, a lab coat, and goggles. As with HF handling, extreme care should be taken because of the toxicity and corrosiveness of the solution. All inhalation, ingestion, and skin and eye contact should be strictly avoided. Etching of silicon wafers should be conducted in a ventilated fume hood using proper double-layered nitrile gloves, a lab coat, and goggles. HF solution spills and burns should be neutralized and treated with 2.5% calcium gluconate gel.

RESULTS AND DISCUSSION

Coupling Spray Deposition with NIMS. The use of spray deposition for sample application with MALDI has been applied by others to improve homogeneous sample introduction and to reduce shot-to-shot variability.⁴² Spray deposition of cations, however, to uniformly enhance ionization has not yet been explored for surface-based MS applications such as biofluid analysis and tissue imaging. In this study, spray deposition of ions on NIMS surfaces was achieved using the configuration shown in Figure 1A. Spray deposition results in the formation of fine, positively charged droplets that dry quickly on the NIMS surface. An important factor in achieving homogeneous ion deposition is spray stability, which is dependent upon a variety of factors including flow rate, the diameter of the capillary tip, the spray solvent, the electric potential, and the distance between the spray tip and the NIMS chip. The best results were achieved with a flow rate of 400 $\mu\text{L}/\text{h}$, a 30- μm diameter tip, a spray voltage of 3 kV, analyte solutions of 50% methanol in water, and a separation distance of ~30 mm between the capillary tip and the NIMS chip. To facilitate uniform deposition over the entire surface of the NIMS chip, we used a computer-controlled X–Y stage that mechanically moved the NIMS chip (Figure 1B).

(42) Hensel, R. R.; King, R. C.; Owens, K. G. *Rapid Commun. Mass Spectrom.* **1997**, *11*, 1785–1793.

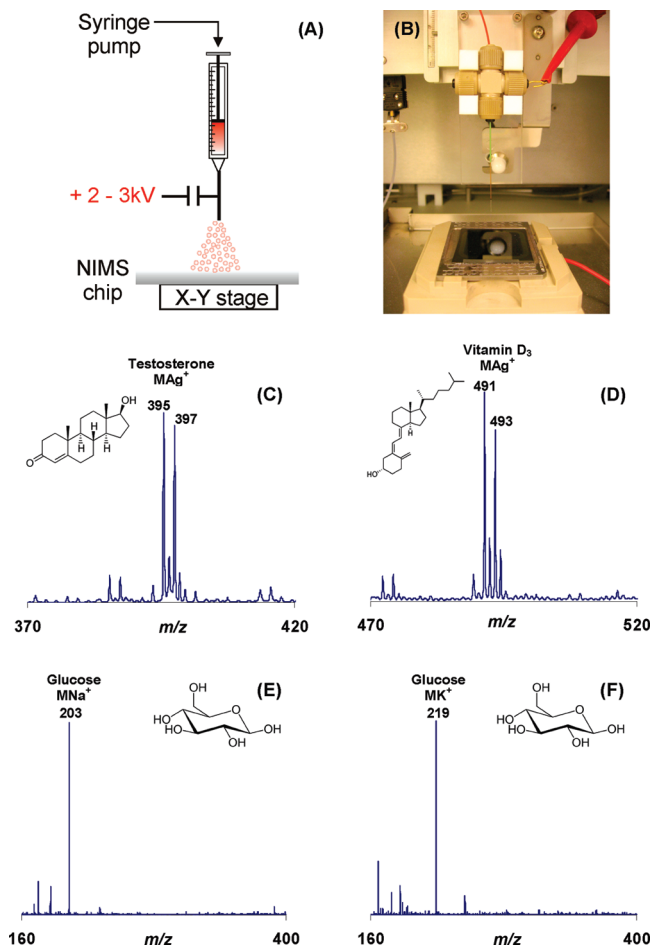


Figure 1. (A) Schematic diagram of the spray-deposition setup. (B) Photograph showing the spray-deposition system. NIMS spectra of (C) testosterone and (D) vitamin D₃ at 300 fmol with spray deposition of AgNO₃. NIMS spectra of glucose at 300 fmol with spray deposition of (E) NaCl and (F) KCl.

Carbohydrates and steroids generally do not ionize in protonated form (MH⁺) and therefore typically cannot be detected using traditional NIMS or other surface-based approaches. Instead, both carbohydrates and steroids are preferably cationized by metal ions.^{30,43,44} Sodium adducts (MNa⁺) are formed by carbohydrates, and silver adducts (MAg⁺) are formed by steroids. Spray deposition of NaCl or AgNO₃ on the NIMS surface provides a source for cationization. Figure 1C,D displays the NIMS spectrum of testosterone and vitamin D₃ at 300 fmol using the silver-enhanced NIMS technique, respectively. We observed [testosterone + Ag⁺] at *m/z* 395 and 397, and [vitamin D₃ + Ag⁺] at *m/z* 491 and 493. The peaks are characterized by a unique isotope pattern because of the naturally occurring silver isotopes (¹⁰⁷Ag and ¹⁰⁹Ag). Figure 1E shows the mass spectrum of glucose at a concentration of 300 fmol. The mass spectrum is dominated by sodium adducts of glucose at *m/z* 203. In comparison, the signal corresponding to potassiated glucose at *m/z* 209 is small because of the excess sodium present. To illustrate the flexibility of the cationization process, we prepared a potassium-rich surface using KCl solution

with identical spray-deposition conditions. Figure 1F shows the NIMS spectrum of glucose with potassium as the spray-deposited metal. In contrast to Figure 1E, the signal from potassiated glucose at *m/z* 219 dominates the spectrum without an observable peak at *m/z* 203. This method for ionizing carbohydrates demonstrates the flexibility of NIMS to detect molecules that undergo specific cationization.

Detection of Carbohydrates using NIMS. One of the most challenging aspects in MALDI analysis of oligosaccharides is the low-ionization efficiency of carbohydrates. It is well established that most carbohydrates ionize via Na⁺ or K⁺ adducts.²⁸ Given that the ionization efficiency of carbohydrates is generally higher with Na⁺ adducts relative to K⁺ and other alkali metals,²⁸ all the carbohydrate analyses presented here were performed using Na⁺ as the cationization metal. Spray depositing excess amounts of NaCl (~3 μmol/chip) provides a rich-sodium cationization source without removal of metal impurities, which may be present at low levels depending on the sample analyzed. Figure 2A displays the NIMS spectra obtained from a mixture of sucrose and maltotriose (500 fmol and 800 amol each). The ion signals at *m/z* 365 and 527 correspond to the sodiated ions of sucrose and maltotriose, respectively. Potassium adducts are not observed due to the much greater concentration of Na⁺ relative to K⁺ ions present on the surface. In addition to small-molecule carbohydrates, higher mass oligosaccharides with different structures were also tested. Specifically, we examined malto-oligosaccharides (maltohexaose and maltoheptaose) and cyclic oligosaccharides (β- and γ-cyclodextrin) given their clinical value in measuring α-amylase activity in human serum and urine.^{43,45} The successful detection of these oligosaccharides highlights the potential use of NIMS as an assay for measuring enzymatic activity.⁴⁶ Figure 2B,C shows the NIMS spectrum of a maltohexaose and maltoheptaose mixture (50 fmol each) and a β- and γ-cyclodextrin mixture (500 amol each), respectively. It is interesting to note that cyclic oligosaccharides are detected with substantially higher sensitivity than malto-oligosaccharides. The higher ionization efficiency of cyclodextrin relative to malto-oligosaccharides is probably due to the larger number of hydroxyl groups present in the center of the cyclodextrin structure capable of forming sodium adducts.⁴⁷

Quantitative Analysis of Human Serum Glucose. We further extended our analysis of carbohydrates using cation-enhanced NIMS to investigate glucose in human serum. Molecules greater than 10 kDa in human serum were removed by a microfilter under centrifugation at 12 000*g* for 30 min. The filtered serum was then diluted 100 times in nanopure water. Quantitative analysis of glucose was performed using the standard-addition method with glucose ¹³C₆ as an internal standard. Typically, 1 μL of the serum sample was spotted on the NIMS surface and air-dried. A calibration curve of glucose was obtained by plotting the ratio of the peak at *m/z* 203 to the peak at *m/z* 209 as a function of spiked-glucose concentration. Depending on metabolism and fasting, normal levels of glucose in human blood

(45) Abe, A.; Tonozuka, T.; Sakano, Y.; Kamitori, S. *J. Mol. Biol.* **2004**, *335*, 811–822.

(46) Northen, T. R.; Lee, J. C.; Hoang, L.; Raymond, J.; Hwang, D. R.; Yannone, S. M.; Wong, C. H.; Siuzdak, G. *Proc. Natl. Acad. Sci. U.S.A.* **2008**, *105*, 3678–3683.

(47) Choi, S. S.; Lee, H. M.; Jang, S.; Shin, J. *Int. J. Mass Spectrom.* **2009**, *279*, 53–58.

(43) Yang, S. J.; Lee, H. S.; Kim, J. W.; Lee, M. H.; Auh, J. H.; Lee, B. H.; Park, K. H. *Carbohydr. Res.* **2006**, *341*, 420–424.

(44) Chiu, T. C.; Chang, L. C.; Chiang, C. K.; Chang, H. T. *J. Am. Soc. Mass Spectrom.* **2008**, *19*, 1343–1346.

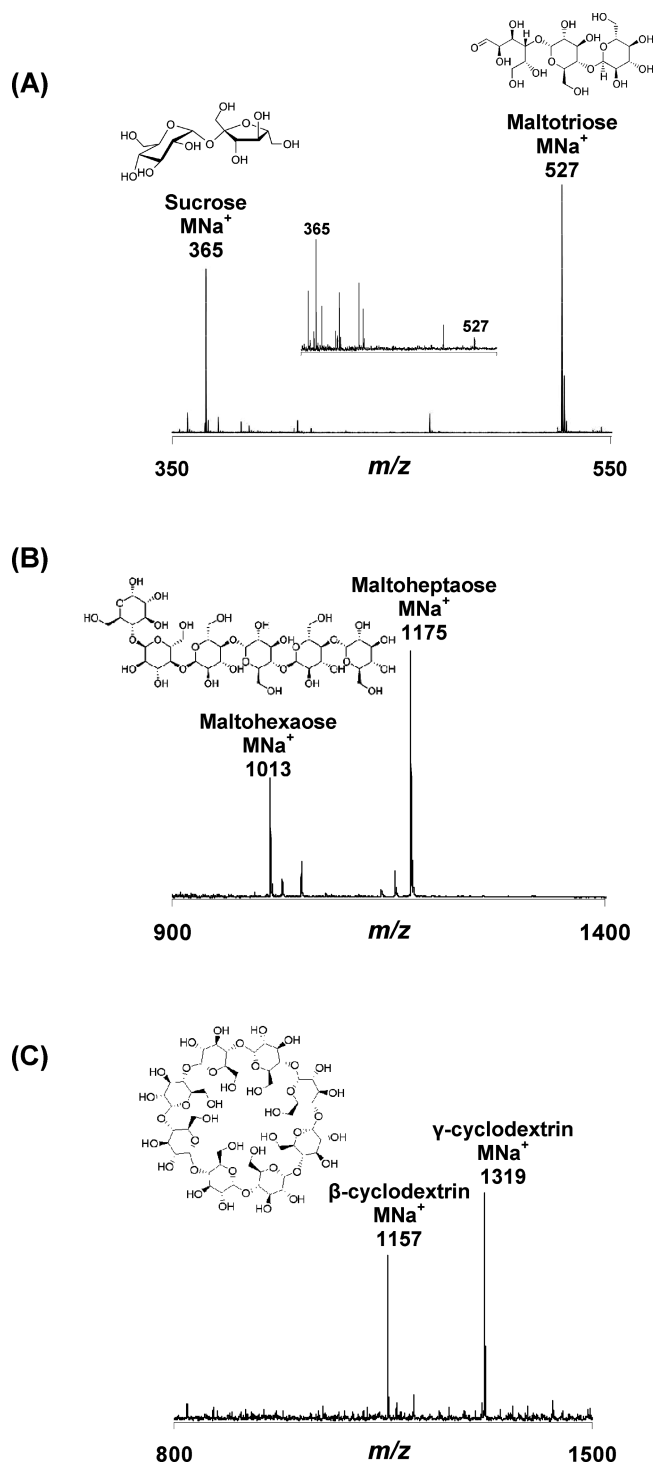


Figure 2. Sodium-enhanced NIMS spectra of oligosaccharides. (A) Mixture of sucrose and maltotriose at 500 fmol each. The inset shows data acquired from a mixture of sucrose and maltotriose at 800 amol each. The atypically high background of the inset is a result of the low concentration of analyte measured. (B) Mixture of the malto-oligosaccharides maltohexaose and maltoheptaose at 50 fmol each. (C) Mixture of the cyclic oligosaccharides β - and γ -cyclodextrin at 500 amol each. The data were acquired using NaCl coated NIMS chips with BisF17 as the initiator.

range from 70 to 125 mg/dL.⁴⁸ The calibration curve of glucose in human serum measured by cation-enhanced NIMS showed good linearity ($R^2 = 0.9975$) in the working range 1–200 μ M

(48) Arky, R. A. *New Engl. J. Med.* **2005**, *353*, 1511–1513.

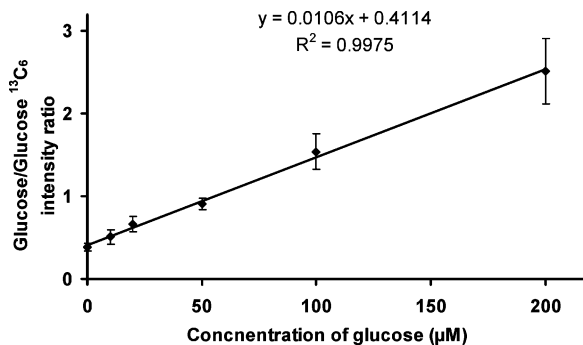


Figure 3. Calibration curve of glucose in human serum using glucose $^{13}C_6$ as an internal standard. The curve was obtained by plotting the ratio of the peak at m/z 203 [glucose + Na^+] to the peak at m/z 209 [glucose $^{13}C_6$ + Na^+]. Error bars were determined from the standard deviation of 10 individual measurements. Note that error bars increase with glucose concentration.

(Figure 3). From the calibration plot, the concentration of glucose in standard human serum obtained from Sigma-Aldrich was estimated to be 4.1 mM (\sim 74 mg/dL), which is within the normal concentration range listed above. The results show the applicability of cation-enhanced NIMS to quantitatively analyze small metabolites in complex biological matrices.

Imaging Sucrose from a *Gerbera jamesonii* Stem. Sucrose is considered to be a key sugar in plant life that plays a crucial role in photosynthesis, nutritional transport, development, storage, and signal transduction.^{48–52} Accordingly, sucrose metabolism is fundamental to plant biology, and monitoring changes in the spatial localization of this carbohydrate (as well as others) offers important insight into plant physiology.

Sodium-enhanced NIMS was used to image the sucrose distribution of a *Gerbera jamesonii* flower stem to demonstrate the applicability of the approach in investigating plant metabolism. Figure 4A shows an optical image of the cross-section of the stem mounted on the NIMS surface. Both sodium and potassium adducts of sucrose were observed in the mass spectrum. The potassium adducts of sucrose are relatively strong because potassium is one of the essential macronutrients in plants.⁵³ The distribution of sucrose [MNa^+ m/z 365] is displayed in Figure 4B. Sucrose was found to be highly localized in the vascular cambium but was also detected at a lower concentration in the phloem. As expected, however, sucrose was almost entirely absent in the xylem. The differential distribution of sucrose is consistent with the observation that sucrose metabolism mainly occurs in the vascular cambium region.^{49,52}

Detecting Steroids Using NIMS. Steroids are another class of molecules that are not effectively ionized by electrospray or MALDI because they lack a site for protonation or deprotonation. The use of silver for HPLC analysis of olefins has been well established given the preference of silver binding to double bonds.⁵⁴ Recently, silver nanoparticles have been used as a matrix for selective ionization of olefinic and cuticular wax compounds

(49) Koch, K. *Curr. Opin. Plant Biol.* **2004**, *7*, 235–246.

(50) Borisjuk, L.; Walenta, S.; Rolletschek, H.; Mueller-Klieser, W.; Wobus, U.; Weber, H. *Plant J.* **2002**, *29*, 521–530.

(51) Farrar, J.; Pollock, C.; Gallagher, J. *Plant Sci.* **2000**, *154*, 1–11.

(52) Sung, S. J. S.; Kormanik, P. P.; Black, C. C. *Tree Physiol.* **1993**, *12*, 243–258.

(53) Maathuis, F. J. M.; Sanders, D. *Physiol. Plant.* **1996**, *96*, 158–168.

(54) Morris, L. J. *Lipid Res.* **1966**, *7*, 717–732.

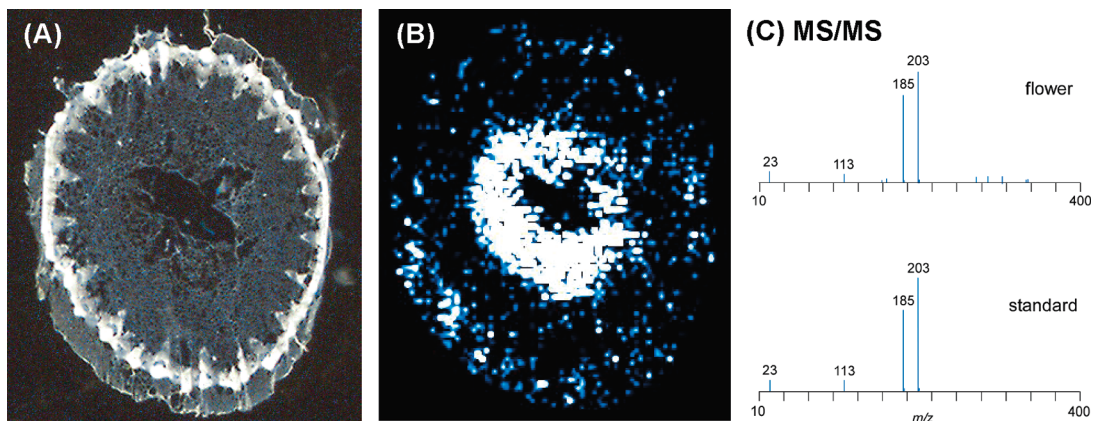


Figure 4. NIMS imaging of a *Gerbera jamesonii* flower stem. (A) Optical image of the stem mounted on the NIMS surface: X, xylem; VC, vascular cambial; P, phloem. (B) Corresponding sucrose [MNa^+ m/z 365] distribution as obtained from sodium-enhanced NIMS. (C) MS/MS data from the flower stem and a commercial standard to confirm the identification of sucrose.

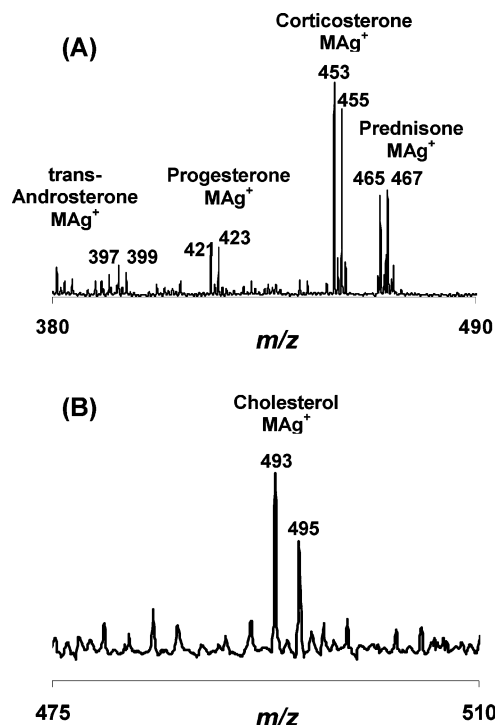


Figure 5. Silver-enhanced NIMS spectra of steroids. (A) Mixture of trans-androsterone, progesterone, corticosterone, and prednisone (500 fmol each). (B) High-sensitivity measurements of cholesterol at 100 fmol. The data were acquired using $AgNO_3$ coated NIMS chips with APDMES as the initiator.

in MALDI experiments.^{55,56} Here we explore the deposition of $AgNO_3$ ions on a NIMS surface for enhancing the detection of steroids. When preparing the steroid solutions to be spotted on the NIMS chips, chloroform was used because steroids are generally not soluble in water. Although BisF17 is generally used as the initiator in NIMS experiments, nonpolar solvents such as chloroform spread out on the BisF17 surface, thereby lowering the experimental sensitivity. Thus, we chose APDMES as an alternative initiator. Spotting chloroform on the APDMES

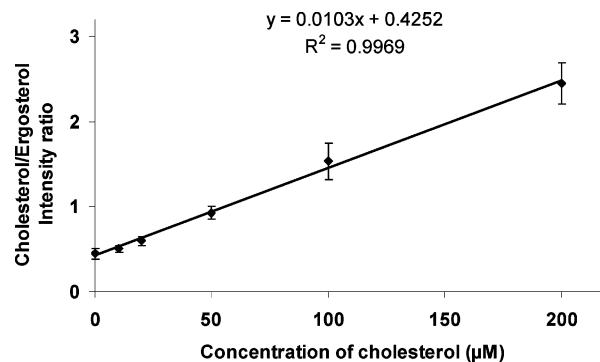


Figure 6. Calibration curve of cholesterol in human serum using ergosterol as an internal standard. The curve was obtained by plotting the ratio of the peak at m/z 493 [cholesterol + Ag^+] to the peak at m/z 503 [ergosterol + Ag^+]. Error bars were determined from the standard deviation of 10 individual measurements. Note that error bars increase with cholesterol concentration.

surface results in less solvent spreading and therefore retains the high-sensitivity characteristic of typical NIMS experiments. Figure 5A shows the NIMS spectrum of a mixture of steroids composed of trans-androsterone, progesterone, corticosterone, and prednisone (500 fmol each) with APDMES initiator. All ions were observed intact as silver adducts (MAg^+). The silver adducts are easy to recognize because of the naturally occurring isotopic pattern of Ag^+ (m/z 107 and 109).

To further examine the utility of silver-enhanced NIMS, we analyzed cholesterol and measured its limit of detection. Figure 5B shows the [cholesterol + Ag]⁺ spectrum (m/z 493 and 495) obtained from the analysis of 100 fmol of cholesterol. These results establish the effectiveness of experimentally modifying NIMS to selectively ionize specific chemical species. For example, metal ions used to capture phosphopeptides from a protein digest could potentially be measured using the NIMS approach described here.^{57–61}

(57) Raska, C. S.; Parker, C. E.; Dominski, Z.; Marzluff, W. F.; Glish, G. L.; Pope, R. M.; Borchers, C. H. *Anal. Chem.* **2002**, *74*, 3429–3433.

(58) Dunn, J. D.; Watson, J. T.; Bruening, M. L. *Anal. Chem.* **2006**, *78*, 1574–1580.

(59) Zhou, H. J.; Xu, S. Y.; Ye, M. L.; Feng, S.; Pan, C.; Jiang, X. G.; Li, X.; Han, G. H.; Fu, Y.; Zou, H. J. *Proteome Res.* **2006**, *5*, 2431–2437.

(60) Chen, C. T.; Chen, W. Y.; Tsai, P. J.; Chien, K. Y.; Yu, J. S.; Chen, Y. C. J. *Proteome Res.* **2007**, *6*, 316–325.

(55) Sherrod, S. D.; Diaz, A. J.; Russell, W. K.; Cremer, P. S.; Russell, D. H. *Anal. Chem.* **2008**, *80*, 6796–6799.

(56) Cha, S. W.; Song, Z. H.; Nikolau, B. J.; Yeung, E. S. *Anal. Chem.* **2009**, *81*, 2991–3000.

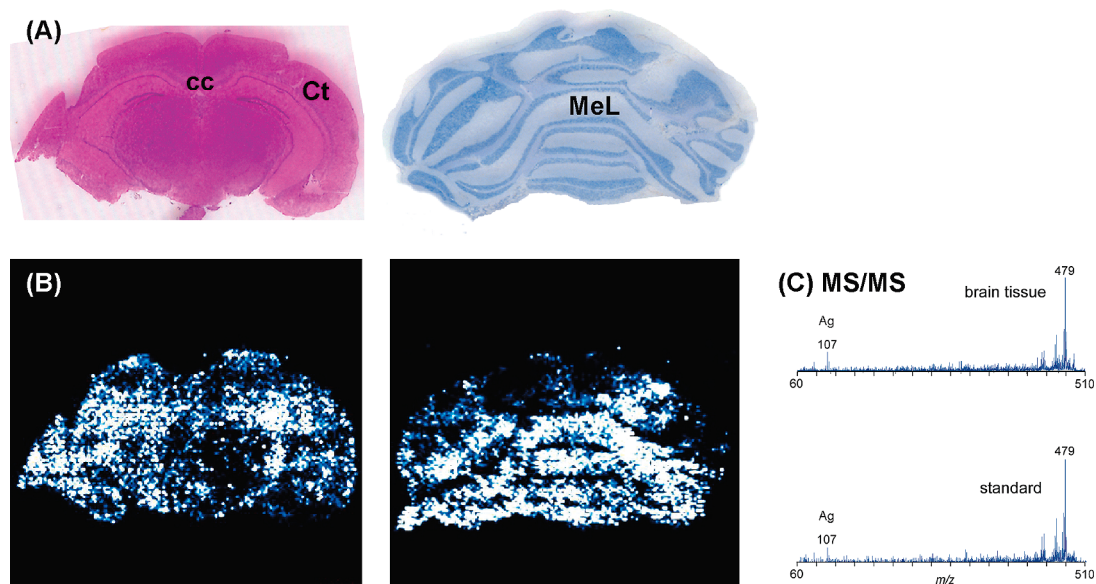


Figure 7. NIMS imaging of a mouse brain. (A) H and E staining showing cortex and corpus callosum (left) and hematoxylin staining showing cerebellum (right) from mouse brain: cc, corpus callosum; Ct, cortex; MeL, medullary layer (white matter). Sections were cut in the coronal orientation. (B) The corresponding cholesterol [Mg^+ m/z 493] distributions as obtained from silver-enhanced NIMS. (C) MS/MS data from mouse brain tissue and a commercial standard to confirm the identification of cholesterol.

Quantitative Analysis of Human Serum Cholesterol. The silver-enhanced NIMS approach for detecting cholesterol was applied to analyze cholesterol in human serum. The American Heart Association recommends a total cholesterol level less than 200 mg/dL to reduce risk of heart disease and stroke.⁶² Human serum (without filtering) was diluted 100 times in nanopure water with ergosterol for an internal standard. A calibration plot of cholesterol was obtained by taking the ratio of the cholesterol peak at m/z 493 to the ergosterol peak at m/z 503 as a function of spiked-cholesterol concentration. The calibration curve of cholesterol in standard human serum obtained from Sigma-Aldrich is plotted in Figure 6. Similar to the glucose calibration plot, a good linearity ($R^2 = 0.9969$) is exhibited in the working range 1–200 μM . The concentration of cholesterol in the standard human serum was estimated to be 4.2 mM (~ 164 mg/dL), which is within the normal recommended cholesterol range. Taken together, the glucose and cholesterol quantification results show the potential applicability of NIMS analysis to the clinical laboratory.

Imaging Intact Cholesterol from Mouse Brain Tissue. Cholesterol is a ubiquitous sterol in healthy brain tissue and an important regulator of lipid organization.⁶³ Defects in cholesterol metabolism, such as those present in Smith–Lemli–Opitz syndrome, severely affect growth, development, and overall brain function.^{64,65} The capacity to obtain high-resolution images of the distribution of cholesterol, particularly in brain tissues, could improve our understanding of normal neurological development and diseases affecting cholesterol metabolism.

Here we used silver-enhanced NIMS to image the distribution of cholesterol in a mouse brain. Cholesterol from a mouse brain has been detected previously using SIMS and LDI-MS; however, the ions observed in these experiments were cholesterol fragments.^{17,22,66–69} Using the NIMS approach described here, we detected and imaged intact cholesterol as silver adducts. Figure 7A shows hematoxylin and eosin (H and E) staining of the corpus callosum and cortex and hematoxylin staining of the cerebellum from mouse brain (cortex and corpus callosum left, cerebellum right). The corresponding cholesterol distributions are displayed in Figure 7B as obtained from silver-enhanced NIMS. Cholesterol was found to be highly localized to the corpus callosum and to the medullary layer of the cerebellum. The results obtained here are consistent with those obtained from previous imaging studies, where cholesterol was concentrated in the white matter.^{17,22,67} In the current case, however, it is important to note that cholesterol was detected as intact ions instead of molecular fragments.

CONCLUSIONS

This study shows the applicability of NIMS to detect compounds that are challenging to observe with traditional MS analysis. Cation-enhanced NIMS is a flexible approach for analyte-specific applications and enables direct analysis of metabolites from complex biological matrices and tissues. In particular, quantitative analysis of glucose and cholesterol from human serum was demonstrated and the potential clinical utility highlighted. The approach was further applied to MS imaging where the

(61) Lo, C. Y.; Chen, W. Y.; Chen, C. T.; Chen, Y. C. *J. Proteome Res.* **2007**, *6*, 887–893.

(62) Wang, T. Y. *Clin. Cardiol.* **2009**, *32*, E22–E28.

(63) Maxfield, F. R.; Tabas, I. *Nature* **2005**, *438*, 612–621.

(64) Tint, G. S.; Irons, M.; Elias, E. R.; Batta, A. K.; Frieden, R.; Chen, T. S.;

Salen, G. *New Engl. J. Med.* **1994**, *330*, 107–113.

(65) Kelley, R. I.; Hennekam, R. C. M. *J. Med. Genet.* **2000**, *37*, 321–335.

(66) Borner, K.; Malmberg, P.; Mansson, J. E.; Nygren, H. *Int. J. Mass Spectrom.* **2007**, *260*, 128–136.

(67) Brunelle, A.; Touboul, D.; Laprevote, O. *J. Mass Spectrom.* **2005**, *40*, 985–999.

(68) McDonnell, L. A.; Piersma, S. R.; Altelaar, A. F. M.; Mize, T. H.; Luxembourg, S. L.; Verhaert, P.; van Minnen, J.; Heeren, R. M. A. *J. Mass Spectrom.* **2005**, *40*, 160–168.

(69) Zheng, L.; McQuaw, C. M.; Ewing, A. G.; Winograd, N. *J. Am. Chem. Soc.* **2007**, *129*, 15730–15731.

distribution of sucrose in a *Gerbera jamesonii* stem and the distribution of cholesterol in a mouse brain were acquired. The data presented here suggest that selecting ions for deposition that bind specifically to unique metabolites may provide new avenues to utilize NIMS for metabolite-specific applications (e.g., targeted metabolomics).

ACKNOWLEDGMENT

Financial support was received from the Department of Energy (Grants FG02-07ER64325 and DE-AC0205CH11231) and the

National Institutes of Health (Grants NIH U54RR025204, 5P30MH062261-08 and R24EY017540). G.J.P. and H.-K.W. contributed equally to this work.

Received for review June 30, 2009. Accepted November 12, 2009.

AC9014353